2020 IEEE/RSJ International Conference on Intelligent Robots and Systems (IROS)
October 25-29, 2020, Las Vegas, NV, USA (Virtual)

Disappearance of chaotic attractor of passive dynamic walking by stretch-bending deformation in basin of attraction

Kota Okamoto[1], Shinya Aoi[1], Ippei Obayashi[2], Hiroshi Kokubu[3], Kei Senda[1], and Kazuo Tsuchiya[1]

Abstract— **Passive dynamic walking is a model that walks down a shallow slope without any control or input. This model has been widely used to investigate how stable walking is generated from a dynamic viewpoint, which is useful to provide design principles for developing energy-efficient biped robots. However, the basin of attraction is very small and thin, and it has a fractal-like complicated shape. This makes it difficult to produce stable walking. Furthermore, the passive dynamic walking shows chaotic attractor through a period-doubling cascade by increasing the slope angle, and the chaotic attractor suddenly disappears at a critical slope angle. These make it further difficult to produce stable walking. In our previous work, we used the simplest walking model and investigated the fractal-like basin of attraction based on dynamical systems theory by focusing on the hybrid dynamics of the model composed of the continuous dynamics with saddle hyperbolicity and the discontinuous dynamics by the impact at foot contact. We elucidated that the fractal-like basin of attraction is generated through iterative stretch and bending deformations of the domain of the Poincaré map by sequential inverse images of the Poincaré map. In this study, we investigated the mechanism for the disappearance of the chaotic attractor by improving our previous analysis. In particular, we focused on the range of the Poincaré map to specify the regions to be stretched and bent by the inverse image of the Poincaré map. We clarified the condition for the chaotic attractor to disappear and the mechanism why the chaotic attractor disappears based on the stretch-bending deformation in the basin of attraction.**

I. INTRODUCTION

Passive dynamic walking is a model that walks down a shallow slope without any control or input [14]. This model has been widely used to investigate how stable walking is generated from a dynamic viewpoint, which is useful to provide design principles for developing energy-efficient biped robots [2], [5], [6], [11]–[13], [22]–[24]. However, the basin of attraction is very small and thin, and it has a fractal-like complicated shape [1], [16], [20]. This makes it difficult to produce stable walking. In addition, the passive dynamic walking shows chaotic attractor through a period-doubling cascade by increasing the slope angle [8], [9]. This makes it further difficult to produce stable walking. Meanwhile, the basin of attraction shows the fractal-like shape even without the period-doubling, which means that fractal-like basin of attraction appears even for single attractor. This indicates that a different mechanism from the period-doubling of the attractor produces the fractal-like basin of attraction, but the mechanism was unclear.

In our previous work [16], [18], we used the simplest walking model [7] for the analysis of passive dynamic walking and elucidated the formation mechanism of the basin of attraction based on dynamical systems theory by focusing on the hybrid dynamics of the model composed of the continuous dynamics during the swing phase with saddle hyperbolicity and the discontinuous dynamics by the impact at foot contact. Specifically, we found that the fractal-like basin of attraction is produced through iterative stretch and bending deformations of the domain of the Poincaré map, which corresponds to the collection of initial conditions from which the model walks at least one step, by sequential inverse images of the Poincaré map.

Although the passive dynamic walking shows chaotic attractor through a period-doubling cascade by increasing the slope angle as explained above, the chaotic attractor suddenly disappears at a critical slope angle. That is, the model no longer continues to walk and falls down, which also makes it difficult to produce stable walking. The mechanism for the disappearance of the chaotic attractor was explained by the boundary (attractor) crisis [10], where the chaotic attractor contacts the boundary of the basin of attraction and disappears [16]. However, because the basin of attraction is the set of all initial conditions that goes to the attractor, the disappearance of the chaotic attractor is equivalent to that of the basin of attraction. The mechanism for vanishing the attractor must be explained by the disappearance of the basin of attraction. In this study, we improved our previous analysis to clarify this vanishing mechanism based on the stretch-bending deformation in the basin of attraction. In particular, we focused on the range of the Poincaré map, which corresponds to the collection of states after the model walked one step starting from the domain, and specified the regions which are stretched and bent by the sequential inverse image of the Poincaré map. Through the analysis of the specified regions, we clarified the condition for the chaotic attractor to disappear and mechanism how the chaotic attractor disappears by the disappearance of the basin of attraction through the stretch-bending deformation.

[1]Kota Okamoto, Shinya Aoi, Kei Senda, and Kazuo Tsuchiya are with the Department of Aeronautics and Astronautics, Graduate School of Engineering, Kyoto University, Kyoto daigaku-Katsura, Nishikyo-ku, Kyoto 615-8540, Japan. shinya_aoi@kuaero.kyoto-u.ac.jp

[2]Ippei Obayashi is with the Center for Advanced Intelligence Project, RIKEN, 1-4-1 Nihonbashi, Chuo-ku, Tokyo 103-0027, Japan.

[3]Hiroshi Kokubu is with the Department of Mathematics, Graduate School of Science, Kyoto University, Kitashirakawa Oiwakecho, Sakyo-ku, Kyoto 606-8502, Japan.

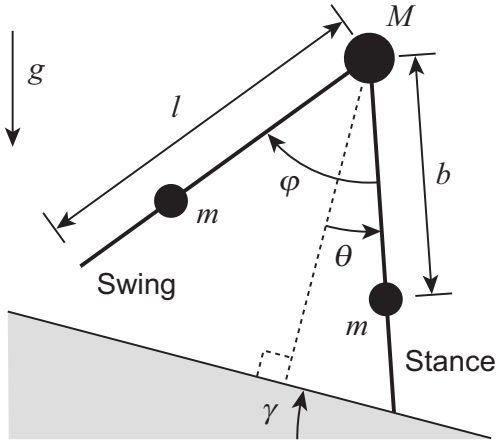

Fig. 1. Compass-type model composed of three mass points and two massless legs for analysis of passive dynamic walking.

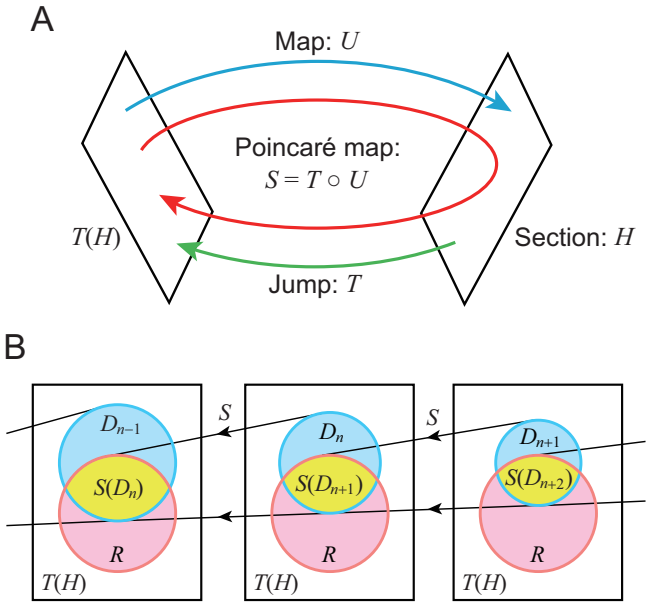

Fig. 2. A. Schematic structure of phase space and B. schematic relationship between D_n, $S(D_n)$, and R on $T(H)$.

II. DYNAMIC CHARACTERISTICS IN PASSIVE DYNAMIC WALKING

A. Model

We used a compass-type model (Fig. 1), which has two legs (length: l) connected by a frictionless hip joint. θ is the angle of the stance leg with respect to the slope normal, and φ is the relative angle between the stance and swing legs. The mass is located only at the hip and the leg (hip mass: M, leg mass: m). The leg mass is located at b from the hip joint. g is the acceleration due to gravity. This model walks on a slope of angle γ without any control or input.

In this study, we focused on the simplest walking model, where $m/M \to 0$ and $b/l \to 1$ [7], because the dynamical characteristics in the passive dynamic walking remain almost unchanged [16]. For example, even when this extreme case is not assumed, the period-doubling cascade produces chaotic attractor and fractal-like basin of attraction appears without the period-doubling [1]. Furthermore, the chaotic attractor suddenly disappears over a critical slope angle.

B. Governing equations

This model is governed by hybrid dynamics composed of the continuous dynamics by the equations of motion during the swing phase and the discontinuous dynamics by the impact at foot contact. The equations of motion are given by

$$\ddot{\theta} - \sin(\theta - \gamma) = 0 \tag{1}$$

$$(\cos\varphi - 1)\ddot{\theta} + \ddot{\varphi} - \dot{\theta}^2 \sin\varphi + \sin(\varphi - \theta + \gamma) = 0 \tag{2}$$

These equations are nondimensionalized by the time scale $\sqrt{l/g}$ and have an equilibrium point at $[\theta\, \dot{\theta}\, \varphi\, \dot{\varphi}] = [\gamma\, 0\, 0\, 0]$. The eigenvalues of the linearized equations of motion at the equilibrium point are ± 1 and $\pm i$, and the equilibrium point is a saddle-centre.

The foot contact occurs when the following conditions are satisfied.

$$2\theta - \varphi = 0 \tag{3}$$

$$-\pi/2 < \theta < 0 \tag{4}$$

$$2\dot{\theta} - \dot{\varphi} < 0 \tag{5}$$

The impact at foot contact gives the following relationship.

$$\begin{bmatrix} \theta^+ \\ \dot{\theta}^+ \\ \varphi^+ \\ \dot{\varphi}^+ \end{bmatrix} = \begin{bmatrix} -\theta^- \\ \dot{\theta}^- \cos 2\theta^- \\ -2\theta^- \\ \cos 2\theta^- (1 - \cos 2\theta^-)\dot{\theta}^- \end{bmatrix} \tag{6}$$

where $*^-$ and $*^+$ are the state $*$ just before and after the foot contact, respectively. Note that the state just after foot contact $[\theta^+\, \dot{\theta}^+\, \varphi^+\, \dot{\varphi}^+]$ depends only on $[\theta^-\, \dot{\theta}^-]$ and is independent of $[\varphi^-\, \dot{\varphi}^-]$.

C. Structure of phase space by hybrid dynamics

This hybrid dynamic system determines the structure of the phase space, as shown in Fig. 2A. H is the section defined by the foot contact conditions (3)-(5). T is the jump from the state just before foot contact to the state just after foot contact, defined by the relationship (6). Therefore, $T(H)$ is the region representing all states just after foot contact and a new step starts from $T(H)$. U is the map from the start of a step to the next foot contact. That is, U is the map from $T(H)$ to H, defined by the equations of motion (1) and (2). The Poincaré section is defined by $T(H)$, on which each state is uniquely determined by two variables $[\theta\, \dot{\theta}]$, and the Poincaré map S is defined by $S = T \circ U : T(H) \to T(H)$. S represents walking one step, and the attractor of S represents

stable walking. S is parametrized by one parameter γ. In particular, S has an attracting fixed point at $0 < \gamma < 0.015$, and there is a period-doubling cascade to chaos for $0.015 < \gamma < 0.019$ [7].

D. Relationship between domain and range of Poincaré map and basin of attraction

We define D_n $(n = 1, 2, \ldots)$ as the collection of initial conditions on the Poincaré section $T(H)$ from which the model walks at least n steps. This satisfies $D_{n+1} \subseteq D_n$ (Fig. 2B). Because the Poincaré map S represents walking one step, $S(D_n)$ explains the state on $T(H)$ after the model walked one step starting from D_n. Because the model can walk at least $n-1$ from $S(D_n)$, $S(D_n) \subseteq D_{n-1}$. Because the domain D of S on $T(H)$ represents the collection of initial conditions on $T(H)$ from which the model walks at least one step, D is identical to D_1.

Using the inverse image of S, we can write $D_n = S^{-1}(D_{n-1})$. However, the inverse image S^{-1} acts only on a part of D_{n-1}, as shown in Fig. 2B. In particular, because $S(D_n) = D_{n-1} \cap R$, where R is the range of S on $T(H)$ and corresponds to the collection of states after the model walked one step starting from the domain D_1, we use $D_n = S^{-1}(D_{n-1} \cap R)$ instead of $D_n = S^{-1}(D_{n-1})$. In the same way, we use $D_n = S^{-1}(S^{-1}(\ldots(S^{-1}(D_1 \cap R) \cap R)\ldots \cap R) \cap R)$ instead of $D_n = S^{-n+1}(D_1)$. Because the model walks at least n steps from D_n, D_n approximates the basin of attraction as n increases.

E. Formation of basin of attraction through stretch-bending deformation by S^{-1}

Because the basin of attraction is approximated by $D_n = S^{-1}(S^{-1}(\ldots(S^{-1}(D_1 \cap R) \cap R)\ldots \cap R) \cap R)$ as $n \to \infty$, it is obtained by the iterative processes to extract the intersection with the range R of the Poincaré map S and to apply the inverse image S^{-1} starting from D_1, which is the domain of S and corresponds to the region from which the model walks at least one step. In our previous work [16], we elucidated that when the inverse image S^{-1} is applied to a region, it is stretched and bent to form a V-shaped region due to the hybrid dynamics of the model composed of the continuous dynamics with saddle hyperbolicity and the discontinuous dynamics by the impact at foot contact. That is, D_1 is stretched and bent many times to create slits and fractal-like basin of attraction is generated, as shown in the schematic processes to deform D_1 in Fig. 3.

Figure 4 shows R, D_1, D_2, D_3, and the basin of attraction for $\gamma = 0.0187 < 0.019$, where $\theta + \dot{\theta}$ and $\theta - \dot{\theta}$ are used for the axes to clarify the geometric characteristics, as used in our previous work [16], [18]. Chaotic attractor appears through the period-doubling cascade. As shown in Fig. 3, D_2 and D_3 are stretched and bent to form V-shaped regions and produce slits. Through the iterative processes, the basin of attraction has a lot of slits, and it shows a fractal-like complicated shape.

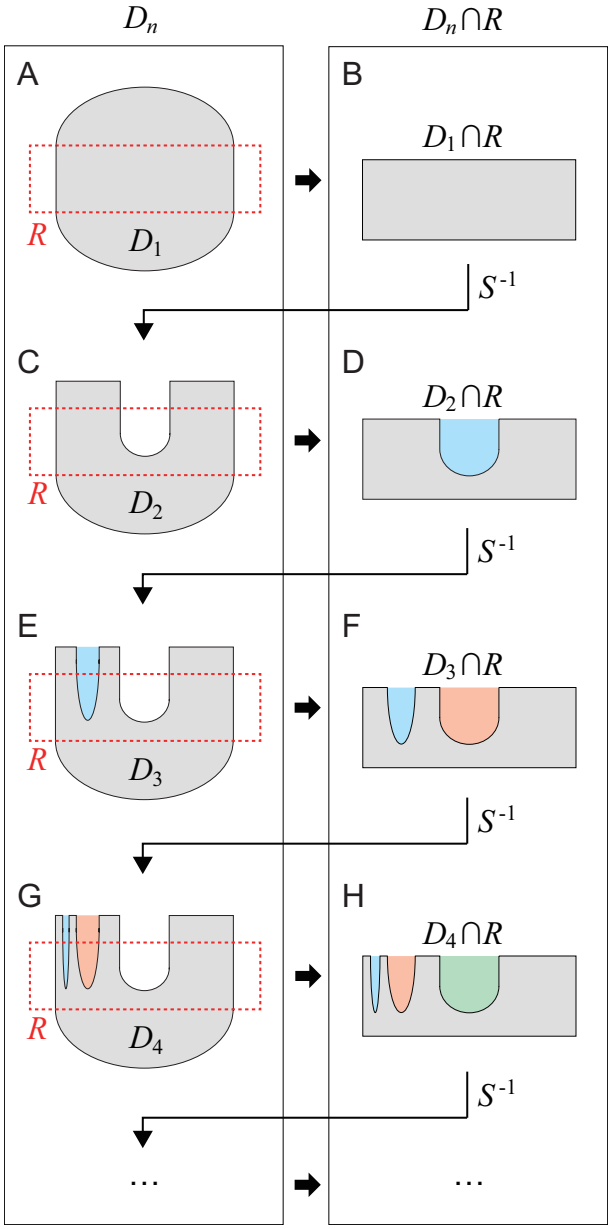

Fig. 3. Schematic processes to deform D_1 to D_2, D_3, and D_4 and generate slits. $D_1 \cap R$ is extracted from A in B, which is stretched and bent by S^{-1} to form D_2 and has one slit in C. In the same way, $D_2 \cap R$ is extracted in D, which is stretched and bent by S^{-1} to form D_3 and has two slits in E. $D_3 \cap R$ is extracted in F, which is stretched and bent by S^{-1} to form D_4 and has three slits in G. The basin of attraction has many slips through these processes.

III. DISAPPEARANCE OF CHAOTIC ATTRACTOR

As described above, the chaotic attractor vanishes when $\gamma > 0.019$. Figure 5 shows R, D_1, D_2, and D_3 for $\gamma = 0.021 > 0.019$, where $\theta + \dot{\theta}$ and $\theta - \dot{\theta}$ are used for the axes to clarify the geometric characteristics. D_1, D_2, and D_3 are not so much different from those for $\gamma = 0.0187 < 0.019$ in Fig. 4.

As compared between Figs. 4 and 5, D_2 and D_3 have almost no difference between before and after the chaotic attractor disappeared. However, they have both V-shaped regions due to the stretch-bending deformation and the inner

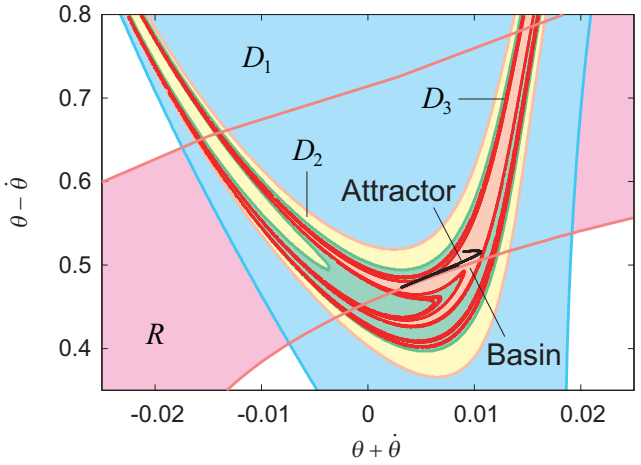

Fig. 4. R, D_1, D_2, D_3, and the basin of attraction for $\gamma = 0.0187 < 0.019$. $\theta + \dot{\theta}$ and $\theta - \dot{\theta}$ are used for the axes to clarify the geometric characteristics.

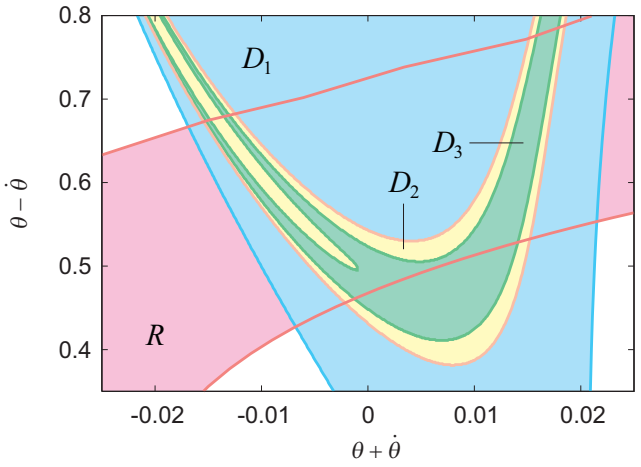

Fig. 5. R, D_1, D_2, and D_3 for $\gamma = 0.021 > 0.019$, where the basin of attraction disappears. $\theta + \dot{\theta}$ and $\theta - \dot{\theta}$ are used for the axes to clarify the geometric characteristics.

edge of the V-shape gets deeper from D_2 to D_3. Because $D_{n+1} \subseteq D_n$, it is possible that the inner edge gets deeper as n increases to reach and penetrate R. Here, we consider the cases where the inner edge penetrates R for the first time at $n = N$, as shown in Fig. 6A (there may be multiple slits in D_N, but because they do not affect the explanation below, they are not shown in Fig. 6). In the same way as that in Fig. 3, the iterative processes to extract the intersection with R and to apply the inverse image S^{-1} are performed to D_N. Because the inner edge of D_N penetrates R (Fig. 6A), $D_N \cap R$ has one penetrating slit (Fig. 6B). Through the stretch and bending deformation, D_{N+1} has one penetrating slit inside the V-shaped region (Fig. 6C). As a result, $D_{N+1} \cap R$ has another penetrating slits at both sides of the penetrating slit of $D_N \cap R$ (Fig. 6D). Through the stretch and bending deformation, D_{N+2} has three penetrating slits inside the V-shaped region (Fig. 6E). As a result,

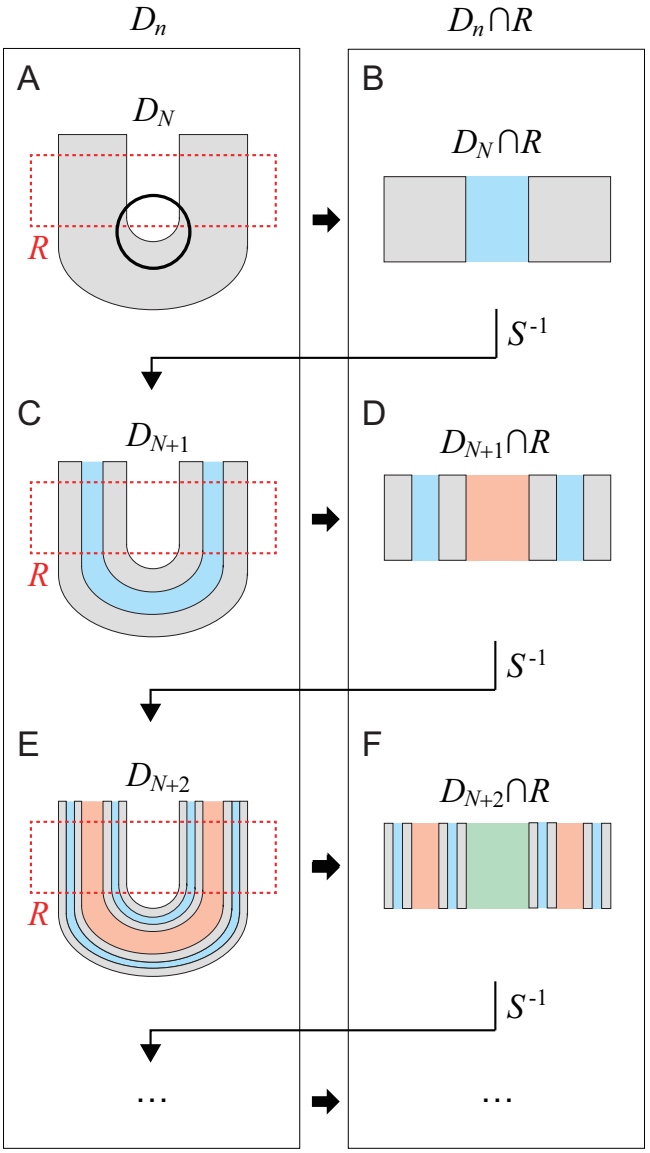

Fig. 6. Schematic processes to deform D_n and generate penetrating slits after inner edge of V-shaped D_n penetrates R for the first time at $n = N$ in A. $D_N \cap R$ has one penetrating slit in B. D_{N+1} has one penetrating slit inside V-shaped region in C. $D_{N+1} \cap R$ has another penetrating slits at both sides of the penetrating slit of $D_N \cap R$ in D. D_{N+2} has three penetrating slits inside V-shaped region in E. $D_{N+2} \cap R$ has another penetrating slits at both sides of two penetrating slits generated at $D_{N+1} \cap R$ in F. $D_n \cap R$ can be assumed as one-dimensional Cantor set.

$D_{N+2} \cap R$ has another penetrating slits at both sides of the two penetrating slits generated at $D_{N+1} \cap R$ (Fig. 6D). By repeating these processes, thousands of penetrating slits are generated. Because $D_{n+1} \subseteq D_n$, $D_n \cap R$ can be assumed as one-dimensional Cantor set [21]. Therefore, $D_n \cap R$ is vanishing as n increases and it disappears.

Figures 7A-E show D_5-D_9, respectively, for $\gamma = 0.021 > 0.019$. The inner edge of the V-shaped D_n penetrates R for the first time at $n = 6$ (Fig. 7B), as shown in Fig. 6A (strictly speaking, the inner edge of a penetrating slit near the inner edge of D_n penetrates R, which induces the same phenomena as the inner edge of D_n penetrates R). As a

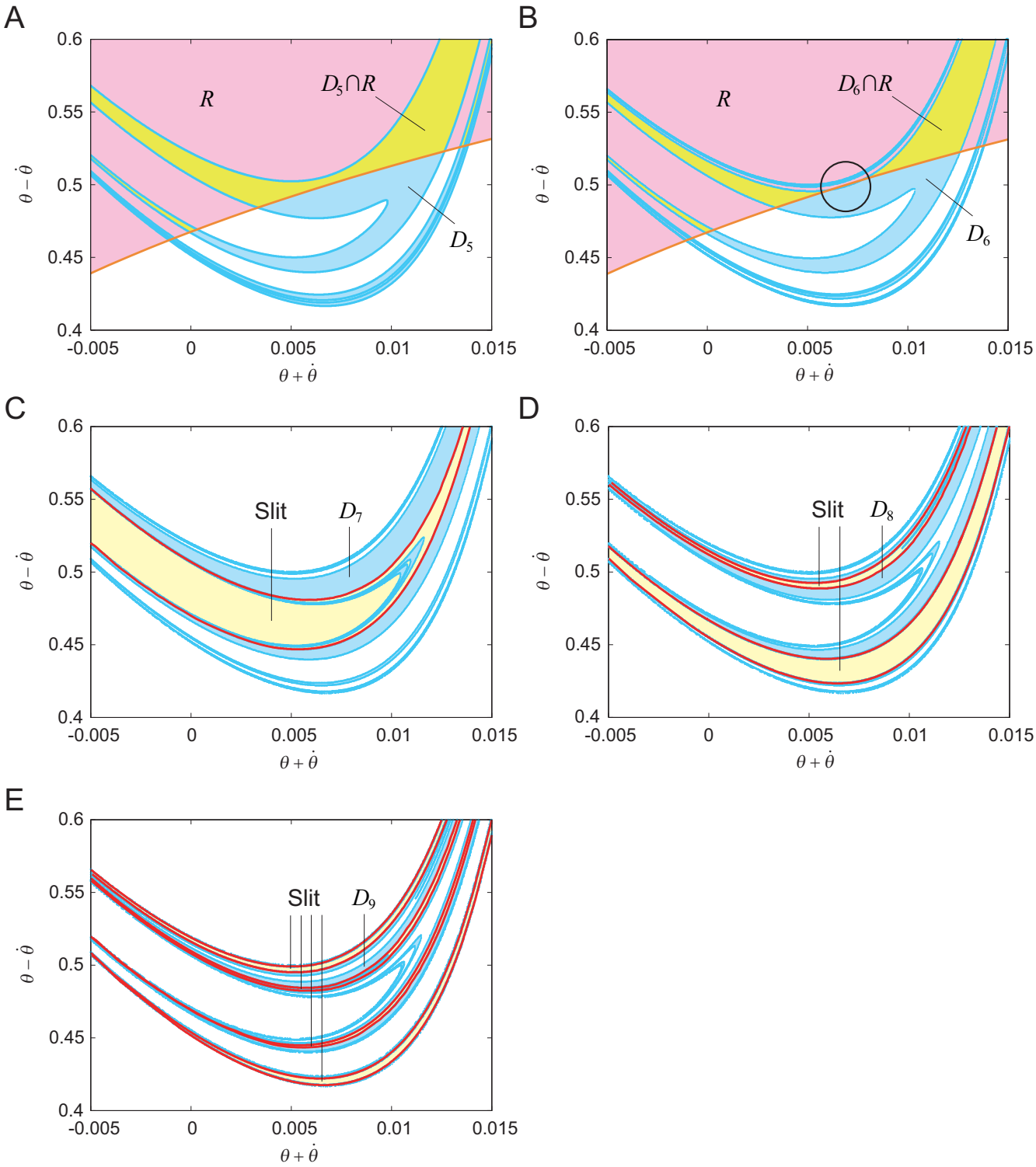

Fig. 7. A-E show D_5-D_9, respectively, for $\gamma = 0.021 > 0.019$. Inner edge of V-shaped D_n penetrates R for the first time at $n = 6$ in B (strictly speaking, inner edge of penetrating slit near inner edge of D_n penetrates R, which induces the same phenomena as inner edge of D_n penetrates R). D_7 has a penetrating slit inside V-shaped region in C. D_8 and D_9 have another penetrating slits at both sides of the generated penetrating slits in D and E, respectively. After inner edge of D_n penetrates R, R is not shown (C, D, and E).

result, D_7 has a penetrating slit inside the V-shaped region (Fig. 7C), as shown in Fig. 6C. D_8 and D_9 have another penetrating slits at both sides of the generated penetrating slits (Figs. 7D and E), as shown in Figs. 6E. D_n gets thinner as n increases. By repeating these processes, the basin of attraction disappears, which also vanishes the chaotic attractor.

IV. CONCLUSION

In this study, we investigated how the chaotic attractor disappears over a critical slope angle in passive dynamic walking using the simplest walking model. In particular, we improved our previous analysis based on dynamical systems theory that clarified fractal-like basin of attraction is generated through the stretch and bending deformation of the domain of the Poincaré map by sequential inverse images of the Poincaré map. We focused on the range of the Poincaré map to specify the regions to be stretched and bent by the inverse image of the Poincaré map, and elucidated that when the inner edge of the V-shaped D_n penetrates the range, the chaotic attractor disappears accompanied by the disappearance of the basin of attraction through the stretch-bending deformation. The period-doubling cascade to chaos appears and the fractal-like basin of attraction is observed even when the simplest case is not assumed [1], [16]. This suggests that similar mechanisms to those observed herein are embedded in general models of passive dynamic walking.

Even when the model is controlled by actuators unlike passive dynamic walking, chaotic attractor appears through a period-doubling cascade by changing model parameters and the chaotic attractor suddenly disappears at a critical value [3], [4], [15]. Furthermore, the basin of attraction is generated through iterative stretch and bending deformations [17], [19]. Therefore, the disappearance mechanism of chaotic attractor exists in many biped robots. Because the disappearance of attractor indicates falling down of the robots, our findings will provide useful design principles for controlling biped robots.

We clarified the mechanism for the disappearance of the chaotic attractor from the disappearance of the basin of attraction. However, the boundary (attractor) crisis [10], which explains the disappearance of the chaotic attractor by the contact with the boundary of the basin of attraction, simultaneously occurs. It remains unclear the mechanism why they occur simultaneously. In addition, when the inner edge of the V-shaped D_n does not penetrate the range, the basin of attraction does not disappear, which also remains unclear. We would like to further improve our analysis to clarify them in the future.

ACKNOWLEDGMENT

This study was supported in part by JSPS KAKENHI Grant Number JP15KT0015.

REFERENCES

[1] Akashi, N., Nakajima, K., and Kuniyoshi, Y. Unpredictable as a dice: Analyzing riddled basin structures in passive dynamic walker. in Proc. Int. Symp. Micro-NanoMechatron. Human Sci., pp. 119-123, 2019.

[2] Asano, F., Luo, Z.-W., and Yamakita, M. Biped gait generation and control based on a unified property of passive dynamic walking. *IEEE Trans. Robot.*, 21:754-762, 2005.

[3] Asano, F. and Luo, Z.-W. Pseudo virtual passive dynamic walking and effect of upper body as counterweight. in Proc. IEEE/RSJ Int. Conf. Intell. Robot. Syst., pp. 2934-2939, 2008.

[4] Aoi, S. and Tsuchiya, K. Bifurcation and chaos of a simple walking model driven by a rhythmic signal. *Int. J. Nonlin. Mech.*, 41(3):438-446, 2006.

[5] Collins, S., Ruina, A., Tedrake, R., and Wisse, M. Efficient bipedal robots based on passive dynamic walkers. *Science*, 307:1082-1085, 2005.

[6] Collins, S.H., Wisse, M., and Ruina, A.. A three-dimensional passive-dynamic walking robot with two legs and knees. *Int. J. Robot. Res.*, 20:607-615, 2001.

[7] Garcia, M., Chatterjee, A., Ruina, A., and Coleman, M. The simplest walking model: Stability, complexity, and scaling. *ASME J. Biomech. Eng.*, 120:281-288, 1998.

[8] Garcia, M., Chatterjee, A., and Ruina, A. Efficiency, speed, and scaling of two-dimensional passive-dynamic walking. *Dynam. Stabil. Syst.*, 15:75-99, 2000.

[9] Goswami, A., Thuilot, B., and Espiau, B.. A study of the passive gait of a compass-like biped robot: Symmetry and chaos. *Int. J. Robot. Res.*, 17:1282-1301, 1998.

[10] Grebogi, C., Ott, E., and Yorke, J.A. Crises, sudden changes in chaotic attractors, and transient chaos. *Physica D*, 7:181-200, 1983.

[11] Hobbelen, D.G.E. and Wisse, M. Swing-leg retraction for limit cycle walkers improves disturbance rejection. *IEEE Trans. Robot.*, 24:377-389, 2008.

[12] Hosoda, K., Takuma, T., Nakamoto, A., and Hayashi, S. Biped robot design powered by antagonistic pneumatic actuators for multi-modal locomotion. *Robot. Auton. Syst.*, 56:46-53, 2008.

[13] Kinugasa, T., Ito, T., Kitamura, H., Ando, K., Fujimoto, S., Yoshida, K., and Iribe, M. 3D dynamic biped walker with flat feet and ankle springs: Passive gait analysis and extension to active walking. *J. Robot. Mechatron.*, 27:444-452, 2015.

[14] McGeer, T. Passive dynamic walking. *Int. J. Robot. Res.*, 9:62-82, 1990.

[15] Narukawa, T., Takahashi, M., and Yoshida, K. Numerical simulations of level-ground walking based on passive walk for planar biped robots with torso by hip actuators. *JSME J. Syst. Des. Dyn.* 2 (2):463-474, 2008.

[16] Obayashi, I., Aoi, S., Tsuchiya, K., and Kokubu, H. Formation mechanism of a basin of attraction for passive dynamic walking induced by intrinsic hyperbolicity. *Proc. R. Soc. A*, 472:20160028, 2016.

[17] Obayashi, I., Aoi, S., Tsuchiya, K., and Kokubu, H. Common formation mechanism of basin of attraction for bipedal walking models by saddle hyperbolicity and hybrid dynamics. *Japan J. Indust. Appl. Math.*, 32(2):315-332, 2015.

[18] Okamoto, K., Aoi, S., Obayashi, I., Kokubu, H., Senda, K., and Tsuchiya, K. Fractal mechanism of basin of attraction in passive dynamic walking. *Bioinspir. Biomim.*, 15(5):055002, 2020.

[19] Okamoto, K., Aoi, S., Obayashi, I., Kokubu, H., Senda, K., and Tsuchiya, K. Investigating phase resetting effect on basin of attraction for walking using a simple model. in Proc 9th Int. Symp. Adapt. Motion Anim. Mach., 2019.

[20] Schwab, A.L. and Wisse, M. Basin of attraction of the simplest walking model. in Proc. ASME Design Eng. Tech. Conf., pp. 9-12, 2001.

[21] Strogatz, S.H. *Nonlinear dynamics and chaos: With applications to physics, biology, chemistry, and engineering*, Perseus Books: New York, 1994.

[22] Sugimoto, Y. and Osuka, K. Hierarchical implicit feedback structure in passive dynamic walking. *J. Robot. Mechatron.*, 20:559-566, 2008.

[23] Wisse, M., Schwab, A.L., van der Linde, R.Q., and van der Helm, F.C.T. How to keep from falling forward: Elementary swing leg action for passive dynamic walkers. *IEEE Trans. Robot.*, 21:393-401, 2005.

[24] Wisse, M., Hobbelen, D.G.E., and Schwab, A.L. Adding the upper body to passive dynamic walking robots by means of a bisecting hip mechanism. *IEEE Trans. Robot.*, 23:112-123, 2007.